Synthesis and spectroscopic characterization of Copper zinc aluminium nanoferrite particles

S. Lakshmi Reddy[1], T. Ravindra Reddy[1], Nivya Roy[2], Reji Philip[2], Ovidio Almanza Montero[3], Tamio Endo[4] and Ray L Frost[5]•

1. Dept. of Physics, SV D.College, Cuddapah 516 003, India.
2. Dept. of Physics, Raman Institute of Science, Bangalore, India
3. Dept. of Physics, Universidad Nacional de Colombia, Bogota D.C.,Colombia.
4. Faculty of Engineering, Mie University, TSU, Mie 514 8507, Japan.
5. School of Chemistry, Physics and Mechanical Engineering, Science and Engineering Faculty, Queensland University of Technology, GPO Box 2434, Brisbane Queensland 4001, Australia.

Abstract

Copper doped zinc aluminium ferrites $Cu_xZn_{1-x.}(Al_xFe_{2-x})O_4$ are synthesized by the solid-state reaction route and characterized by XRD, TEM, EPR and non linear optical spectroscopy techniques. The average particle size is found to be from 35 to 90 nm and the unit cell parameter "a" is calculated as from 8.39 to 8.89 Å. The cation distributions are estimated from X-ray diffraction intensities of various planes. The XRD studies have verified the quality of the synthesis of compounds and have shown the differences in the positions of the diffraction peaks due to the change in concentration of copper ions. TEM pictures clearly indicating that fundamental unit is composed of octahedral and tetrahedral blocks and joined strongly. The selected area electron diffraction (SAED) of the ferrite system shows best crystallinity is obtained when Cu content is very. Some of the d-plane spacings are exactly coinciding with XRD values. EPR spectra is compositional dependent at lower Al/Cu concentration EPR spectra is due to Fe^{3+} and at a higher content of Al/Cu the EPR spectra is due to Cu^{2+}. Absence of EPR spectra at room temperature indicates that the sample is perfectly ferromagnetic. EPR results at low temperature indicate that the sample is paramagnetic, and that copper is placed in the tetragonal elongation (B) site with magnetically non-equivalent ions in the unit cell having strong exchange coupling between them. This property is useful in industrial applications. Nonlinear optical properties of the samples studied using 5 ns laser pulses at 532 nm employing the

• Author to whom correspondence should be addressed (r.frost@qut.edu.au)
* corresponding author email: drslreddy_in@yahoo.com

open aperture z-scan technique indicate that these ferrites are potential candidates for optical limiting applications.

Key words: Copper doped zinc aluminium ferrite, synthesis solid state reaction route, XRD, EPR, non-linear optics, TEM, Tetragonal symmetry.

1. Introduction

The spinel is a mixed metal oxide with a general formula $(M^{2+})(M^{3+})_2(O^{2-})_4$ where M is a transition metal ion or a combination of ions. Many compounds adopt this type of structure. Generally magnetic ferrites are denoted by the formula AB_2O_4 where A and B refer to tetrahedral and octahedral sites respectively in the Fcc oxygen lattice. The unit cell contains eight formula units. Each unit cell consists of eight tetrahedral (A) sites and four octahedral (B) sites in the Fcc lattice. Hence half of the octahedral interstitial sites are occupied by trivalent metal ions and 1/8 of the tetrahedral interstitial sites are occupied by divalent ions in a normal spinel. In A site the divalent metal ion is in the center of a tetrahedron surrounded by four oxygens, whereas in B site the trivalent metal ion is in the center of an octahedron and is surrounded by six oxygens.[1]. The equilibrium distribution of cations in the nano spinel compound structure depends on ionic radii, electronic configuration, chemical composition, method of preparation, grain size, electrostatic/crystal field stabilization energies (CFSE), and polarization effects [2,3]. Cations like Zn^{2+}, Mg^{2+} and Cd^{2+} show a strong preference for the A site, whereas Fe^{3+} ions prefer the B-sites. In inverse spinels cations like Mn^{2+}, Ni^{2+}, Co^{2+}, Cu^{2+} occupy one of the B sites and hence one of the trivalent ion occupies tetrahedral sites thus inverting the structure. It is reported that the method of preparation plays a very important role with regard to the chemical, structural and magnetic properties of spinel ferrites [4].

In general spinels are classified into three types; viz. normal, inverse and mixed spinel. $(Zn/Mg)Fe_2O_4$ is a normal spinel, $(Zn/Mg)(Al/Mn/CrNi/Fe)_2O_4$ is a mixed spinel, and examples of inverse spinel include magnetite, $NiFe_2O_4$ etc., In all inverse spinels one of the trivalent ion is in tetrahedral hole and the divalent metal ion is in the octahedral hole. There are a total of 56 ions in the unit cell of a spinel, of which 8 are M^{2+} ions, 16 are M^{3+} ions and 32 are O^{2-} ions. This is calculated as: 64 tetrahedral A site (8 x 8=64), 32 octahedral B site. Moreover, in normal spinel 8 M^{2+} are in the A site and 16 M^{3+} are in the B site, while in inverse spinel 8 M^{3+} are in the A site, and 8 M^{2+} and 8 M^{3+} are in the B site. In mixed spinels the cation distribution in the A and B sites is not exactly similar to that in the normal and inverse structures. The structural and the magnetic environments of these two sites are quite different from each other.

The substitution of nonmagnetic ions such as Al^{3+} ions in simple and mixed ferrites has received substantial attention over the past few years [5-7]. The introduction of paramagnetic copper is found to enhance the formation of mixed spinels. It has been reported that the presence of nonmagnetic ions reduces magnetic interactions between the two interstitial sites and weakens hyperfine magnetic fields, thereby changing the magnetic and electronic properties. In recent years, research on spinel ferrites has received renewed attention due to the availability of new and sophisticated techniques for the synthesis and characterization of nanoparticles. Normal ferrites are widely used for microwave and non-crystalline (powder) ferrites for high frequency applications but the nano ferrites have several uses in heat transfer devices, drug delivery systems, solar cell applications and medical diagnostics, including cancer treatment. [8,9]. It is well known that when ferrites are sufficiently diluted with non-magnetic atoms they can show a wide spectrum of magnetic structures, ferromagnetic order etc [10]. From an application point of view, it is quite meaningful to investigate how the magnetic and electronic properties and the structure of mixed spinels change by the introduction of paramagnetic and non-magnetic atoms into the lattice. In fact to the best of our knowledge, EPR studies are not reported so far on ferrite systems which contain paramagnetic metal ions. Therefore, in the present work, we have synthesized copper doped zinc aluminum ferrites of nano-size via a solid-state route. XRD, EPR and TEM measurements have been carried out in order to determine the cation distribution in the ferrite system under study. Moreover, open aperture z-scan measurements have been done using 5 ns laser pulses at 532 nm to measure the nonlinear optical transmission of the samples, to calculate the nonlinear absorption coefficient, and estimate their potential for optical limiting applications.

2.Experimental

2.1 Synthesis of nano sized copper doped zinc aluminium ferrite

Samples of the mixed spinel ferrites $(Zn_{1-x}Cu_x)(Al_xFe_{2-x})O_4$ with variable composition (x = 0.15, 0.45, 0.75 and 0.90) are synthesized by using standard solid state route method. Mostly in the synthetic ferrite systems, Zn composition remains constant and is at its regular lattice site while Fe^{3+} was replaced by aluminium. But in the present syntheses composition of all Zn, Cu, Al and Fe ions are changed. All the chemicals used are of analytical grade only. Distilled water is used for the preparation of the required solution. The process is described below:

(i) 2.2886 g of pure zinc granules are dissolved in1:1 HCl and evaporated on sand bath near to dryness and 2.5572 g of $CuCl_2.2H_2O$ is added to it. (ii) An amount of 33.3319 g of ferrous ammonium sulphate is dissolved in 1:1 dilute HCl. Its color becomes very light green and1:1 NH_4OH is added drop wise until the precipitate is formed the color becomes dark green due to the formation of $Fe(OH)_2$. The resulting mixture is stirred continuously for about 2 hours to convert it to $Fe(OH)_3$ by desired oxidation filtered through an ordinary filter paper and washed several times with distilled water. (iii) 2 gm of $Al_2(SO_4)_3$ is weighed and is dissolved in 15 ml of distilled water, 2 gm of NH_4Cl is added and 1:1 NH_4OH is added drop wise until the precipitation is complete. It is filtered and washed thoroughly with distilled water. The three solids are dissolved independently in minimum amount of 1:4 HCl (200 ml of water + 50 ml of HCl). The proportionate weight used in each sample is given Table-1.

All the three solutions are mixed together and 3-5 ml of acetone is added for reducing the particle size is filtered through an ordinary filter paper to remove any insolubles. Final products are dried solutions and then heated up to 400^0C on Bunsen burner. The synthesized final products of nano-size copper doped zinc aluminium ferrites $(Zn_{1-x}\ Cu_x)(Al_xFe_{2-x.}O_4)$ are calcinated in air by raising the temperature up to 200^0C at the rate of 6 ^{0}C/minute in the hot air oven. The dried nano ferrite samples are taken in different silica crucible free from moisture and are then placed in the incinerator of a Muffle Furnace (Biocraft Scientific Systems (P) Ltd, Agra. India). The temperature is raised to 1200 ^{0}C and then allowed to cool to room temperature at the rate of 1^0C/minute in 17 hours. Again the temperature is raised to 1000 ^{0}C in 2 hours and cooled very slowly to room temperature at the rate of 1^0C/minute in 17 hours. The reacted materials in each crucible were well grounded separately in an agate pestle mortar. Now the compounds formed are nano-sized copper doped zinc aluminium ferrite.

2.2 Characterisation Techniques

X-ray powder diffraction patterns of all the samples are recorded using Philips X-ray diffractometer operated in reflection geometry at 30 mA, 40 kV with Cu-K_α (λ = 1.54060 Å). The source is kept at 25 ºC. Data are collected using a continuous scan rate of 1º per 2 min which is then refined into 2 theta steps of 0.02°. The TEM images

are obtained on Philips CM 200 transmission electron microscope operating at 200 kV having a resolution 0.23 nm. EPR spectra of the samples (x= 0.15, 0.45, 0.75 and 0.90) are also recorded from 95 K to 300K on Bruker ESR spectrometer operating at X band frequency (υ =9.45 GHz) having a 100 KHz field modulation to obtain first derivative EPR spectrum. DPPH with a g value of 2.0036 is used for g factor calculation.

2.3 Z-scan measurements

In the open-aperture z-scan technique, essentially the optical transmission of a given sample is measured as a function of the light fluence (energy per unit area) falling on it to ascertain whether the sample shows nonlinear transmission or not. In the typical experimental configuration a Gaussian laser beam is focused using a converging lens, which is a simple way to achieve a continuous variation of laser fluence along the beam axis (taken as the z-axis). The sample is then placed at different positions with respect to the beam focus (z=0), and the corresponding transmissions are measured. The fluence which is a maximum at the focal point will decrease towards either side as given by

$$F(z) = 4\sqrt{\ln 2}\left(\frac{E_{in}}{\pi^{3/2}}\right)\omega(z)^2$$

Here E_{in} is the input laser energy and ω(z) is the beam radius, given by

$$\omega(z) = \omega(o)\sqrt{1+\left(\frac{Z}{Z_0}\right)^2}$$

with ω(0) being the focal spot radius, and $Z_0 = \frac{\pi\omega_{(0)}^2}{\lambda}$ the Rayleigh range (λ is the laser wavelength). In practice the sample is mounted on a linear translation stage to achieve smooth translation with good spatial resolution. By plotting the normalized transmission (T_{norm}) against the sample position (z), the open-aperture z-scan curve is obtained. The above two equations can be used to calculate F(z) for each z so that the variation of T_{norm} with F(z) also can be plotted. Appropriate transmission equations are now used to numerically fit the measured data and estimate nonlinear absorption coefficients. We used the second harmonic output (532 nm) of a Q-switched Nd: YAG laser (Continuum, MiniLite), generating laser pulses of 5 ns duration for the measurements. $(Zn_{1-x}Cu_x)(Al_xFe_{2-x})O_4$ samples with x = 0.15, 0.45, 0.75, and 0.90

were investigated. Samples were dissolved in HCl and taken in a glass cuvette of 1 mm path length. By appropriate dilution the linear transmission of all samples was adjusted to 46% in the 1 mm cuvette. Laser pulse energy used was 70 μJ, and laser pulses were fired at a low repetition rate of 0.2 Hz to the cuvette to avoid sample heating that might otherwise interfere with the measurements. The input energy and the transmitted energy were measured using two pyro-electric energy probes (RjP 735). The z-scan curve plotted from the measured data shows a dip in the focal region indicating nonlinear absorption

3. Results and Discussion

3.1 X-ray diffraction results

Fig.1 presents the X-ray diffraction patterns of all copper doped zinc aluminium ferrite samples recorded on Philips diffractometer up to 25 º. In Fig. 1 all major peaks were indexed to the standard pattern for ferrite, Fe_3O_4. These peaks show the cubic spinel ferrite system. The values of the crystal lattice constant "a" for all the samples determined from X ray data are listed in Table-2. The lattice constant (a) is found to increase linearly with copper/aluminium concentration (x). This indicates that the variation of x with a obey Vegard's law [11]. This behaviour of lattice constant with concentration may be due to substitutional effect of larger Cu^{2+} (0.73) and smaller Al^{3+} (0.50 Å) ions which replace Fe^{3+} (0.64 Å) ions at octahedral (B) site where as Fe^{3+} ions are replaced by Zn^{2+} ions in position. Due to this ionic radii of tetrahedral (A) sub lattice remains same and octahedral (B) sub lattice ionic radii increases. Similar results are observed when composition of Cu is varied in the ferrite system [12]. Further Zn^{2+} and Cu^{2+} ions have strong preference for tetrahedral (A) site and Al^{3+} occupies the octahedral (B) site. The X-ray density 'd_x' is calculated using the formula[13] $d_x = \frac{ZM}{NV^3}$. Here "Z" (8) represents the number of molecules in a unit cell of the nano copper doped zinc aluminium ferrite lattice where M is the molecular weight of the compound, 'N' is the Avogadro's number and 'V is the lattice volume of the sample. The calculated X-ray density for all the samples is also given in Table-2. The density decreases with increase of Cu/Al concentration (x). This is because the increase in composition of Cu/Al content in the spinel system decreases the mass. Also the unit cell volume increasing with increase of doping of Cu/Al content. Hence X ray density decreases.

The average grain size of the compound is evaluated from the line broadening of the peak (311) using Debye - Scherner equation $D_{(hkl)} = \frac{0.9\lambda}{\beta_{1/2}\cos\theta}$ Here D is the average particle size of the crystal, λ is the wavelength of incident X ray, θ is the corresponding Bragg angle , $\beta_{1/2}$ is the full width at the half maximum height (FWHM) of the peak. The average particle size of the ferrite compound is calculated and is given in Table-2.

The cation distribution in the spinel ferrite system has been estimated from X-ray diffraction measurements [14-16]. It has been reported that the intensities of (220), (422) and (440) planes are sensitive to cations on tetrahedral (A^-) and octahedral (B^-) sites [17,18]. The intensity of (222) is very sensitive to octahedral site. Therefore the intensities of (220), (422), and (440) planes are used to determine the cation distribution. The intensity ratios (I_{220}/I_{440} and I_{422}/I_{440}) have been considered to be more sensitive to the cation distribution [19]. It is known that Fe^{3+} and Al^{3+} ions distribute over A^- and B^- sites [20], while Zn^{2+} and Cu^{2+}ions have strong preference for A^-site [21-23]. The intensities corresponding to (220) and (422) reflections are most sensitive to cations on tetrahedral sites [17,18], while those of (333) reflection are sensitive to cation on octahedral sites [17]. The intensity ratios: I_{220}/I_{440}, I_{422}/I_{440} and I_{440}/I_{333} to the samples are calculated. The calculated intensity ratio versus Al/Cu content is shown in Table-3. It is clear that ratio decreases as content increases. The intensity of (222) goes on increasing with Cu content. This suggests that Cu is substituted into octahedral site than tetrahedral site. This suggests that the formation of mixed spinel is very high.

3.2 TEM analysis

TEM was employed to visualize the size, shape and to confirm the nano crystalline nature of the synthesized copper doped zinc aluminium ferrite. Fig.2 shows the typical bright field TEM images of the synthesized $(Cu_xZn_{1-x})(Al_xFe_{2-x})O_4$ nanoparticles. Also it is noticed that the ferrite particles are well defined with polygonal octahedral and tetrahedral shapes. The dense assembly of uniformly sized ferrite nanoparticles are seen at lower concentration of Al/Cu and at higher

concentrations, pale assembly of uniformly sized ferrite nanoparticles are observed. The whole surface of the grid was covered with ferrite nanoparticles. From the Fig.2 it is clear that the ferrite particles had well-defined polygonal growth forms with octahedral and tetrahedral shapes. These two are well joined. This type of joining may find important application as building block for magnetic nanostructures. Further some of the grains are over lapped and could not be identified separately. The grain size of the particles with different Al/Cu concentrations are given in Table-4.

The agglomeration of nano particles is usually explained as a common way to minimize their surface free energy in nano materials [24,25]. It has been observed in the synthesized compounds that the particles prepared with smaller Al/Cu substitution are some what agglomerated in nature. The degree of agglomeration decreases with increasing Al/Cu substitution. The particles prepared from higher Al/Cu concentration are discrete. The decrease in agglomeration is due to the replacement of Fe^{3+} ions by Al^{3+} ions and Zn^{2+} ion by Cu^{2+} ions that leads to decrease in radii of cations involved, which inturn decreases the grain size. Hence the lattice constant decreases. From the Table-4 it can be seen that the mean particle size is 45 nm to 70 nm. The particles at lower Al/Cu concentration in the range 60 nm to 85 nm whereas at higher Al/Cu concentration in the range observed is 30–65nm. Certain particles have a diameter between 150 and 300 nm. The particle sizes range from 30 nm to as high as 300 nm. The particle size distribution is broader and indicates the polycrystalline nature. The average particle sizes estimated from the TEM studies listed in Table -4 are in agreement with those values obtained from XRD analysis.

The selected-area electron diffraction (SAED) pattern of the copper doped zinc aluminium ferrite is also shown in Fig-3. From the Fig.3 the crystal plane d-space is measured and is given Table-4.The ED pattern consists of concentric rings with spots over the rings. This feature indicates that the samples are good nanocrystalline in nature. [26-27]. The rings with a dotted pattern in SAED confirm the wide size distribution of CuO/AlO nano particles. From the Table-4 it is also clear that crystal plane d-spacing is decreasing with increase of Al/Cu concentration. This is in

agreement with the XRD results. As Al/Cu content increases the crystallinity also increases and the best crystal nature is observed at Al/Cu = 0.90 wt%, which is shown in Fig. 3. The ED image clearly shows that the crystal d-plane of (310) and (333) which are well agreeing with the XRD values.

3.2 EPR Spectral results

EPR spectra recorded for copper doped zinc aluminium ferrite system, $Cu_xZn_{1-x}(Al_xFe_{2-x})O_4$ (x= 0.15, 0.45, 0.75 and 0.90), from 95 K to 300 K. These are shown in Fig. 4 as (a), (b) and(c). The analysis is as follows:

Fe^{3+}, a d^5 ion with $^6S_{5/2}$ spin state splits into three Kramers doublets, separated by nearly 1.0 cm^{-1}. In this case, only the lowest doublet is populated and one can observe resonances at g = 9.0 [28,29]. On the other hand, if the middle Kramers doublet is also populated, a g value of 4.29 is expected. If third doublet is also populated, g values ranging from 0.3 to 4.29 can be seen. A few systems are known which exhibit resonances from all the three Kramers doublet [29,30]. In the present case the g value observed at 9.0 and 3.5 can be attributed to the resonance arising from the three Kramers doublets which are populated even at 300K.

(i) EPR spectra of $Cu_{0.15}Zn_{0.85}Al_{0.15}Fe_{1.85}O_4$ recorded from 95K to 300K is shown in Fig. 4(a). At all the temperatures the spectra exhibit two resonant signals one at lower field and another at higher field. Due to high concentration of iron (1.85) and the low copper content (0.15), EPR lines are hidden. Thus the observed two resonant signals are attributed to characteristic of Fe^{3+}. The higher field (around 331.53 mT) resonant signal remains constant, at g=2.04 at all temperatures, whereas the lower field signal approaching higher field signal as the temperature is increased. The higher field signal may be attributed to Fe^{3+} ions on the octahedral (B) site and the lower field signal is attributed to Fe^{3+} ions on the tetrahedral (A) site. Further the resonant field signal at lower end shows, a gradual montonic decrease with increasing temperature. This is due to dipolar-dipolar broadening which decreases with increase in temperature. The g values and area of resonant signals are given Table -5. The ratio of area of resonant signal at higher field to lower field gives the ratio of amount of Fe^{3+}

entering into octahedral (B) and tetrahedral (A) sites which coincides with the calculated value of XRD analysis.

(ii) EPR spectra of $Cu_{0.45}Zn_{0.55}Al_{0.45}Fe_{1.55}O_4$ recorded from 95K to 300K are shown in Fig. 4(b). The overall EPR spectra is symmetric with a single resonant curve with g= 2.04. From the Fig. 4(b) it is noticed that when the temperature increases, the area of the resonant curve decreases and changes the g value. This may be due to the fact that Fe^{3+} ions are only in octahedral B site. In tetrahedral A site the zinc and copper concentrations are almost equal and a very few Fe^{3+} ions may have entered into the lattice. Thus diamagnetic nature of zinc in A site is superimposed on copper and iron ions. Hence lower field resonant signal may be absent.

It is noticed that on increasing the Al^{3+}/Cu^{2+} ions concentration (x), the value of higher field resonance signal remains almost unchanged and lower field signal disapper indicating that S-electron distribution of Fe^{3+} ions have hardly affected by Al^{3+} substitution. Hence the presence of Fe^{2+} ions in the present ferrite system is ruled out. Thus the electron exchange interaction ($Fe^{2+} \leftrightarrow Fe^{3+}+e^-$) does not occur and hence the oxidation state of Fe^{3+} remains unchanged during the synthesis. Further the resonant signal at lower field show a gradual monotonic decrease with increasing Cu/Al concentration (x). This is because of super transferred hyperfine field at the central cation that originates from the magnetic moments of the nearest-neighbor cations, that is, from the intra-sub-lattice contributions h_{AA} and h_{BB} and the inter sub-lattice contributions h_{AB} and h_{BA}. In the present ferrite system, under study, the inter sub-lattice contributions h_{AB} and h_{BA} are predominant. The introduction of Al^{3+} ions replaces Fe^{3+} ions in the A- and B-sites decreases inter sub-lattice contributions, which in turn decreases the hyperfine field H_{hfs} at both A- and B-site. As nonmagnetic Al^{3+} ions replaces Fe^{3+} ions, the correct amount of Fe^{3+} present at A- and B-sites is estimated by determining the area under the EPR spectrum. The correct amount of Fe^{3+} ions occupied by octahedral (B-) and tetrahedral (A-) sites obtained from the EPR spectra and those calculated on the basis of cation distribution are in good agreement. The Fe^{3+}(octahedral site)/Fe^{3+} (tetrahedral site) ratio obtained from the EPR spectra and X-ray intensity calculations

decreases with increasing Cu/Al concentration suggesting the decrease of ferri magnetic behavior. With increase of Cu^{2+}/Al^{3+} ions concentration, intensity and the line width of the EPR spectra increases indicating a reduction in particle size and it is in accordance with TEM measurements. These results are in consistent with the results reported earlier [31].

(iii) EPR spectra of $Cu_{0.75}Zn_{0.25}Al_{0.75}Fe_{1.25}O_4$ recorded from 95K to 300K are shown in Fig. 4©. The spectrum is characteristic of Cu^{2+} in tetragonal distortion. This behaviour is valid upto temperature from 95K to 145K. From the spectrum, the g values obtained are g_{11} = 4.82 to 3.14 and $g_{\perp}$ = 2.04. As the ferrite contains a very high percentage of copper, the hyperfine lines due to Cu(II) could not be resolved. If $g_{11} > g_{\perp}$, the ground state is $^2B_{1g}$, whereas if $g_{\perp} > g_{11}$ or g_{11} = 2.00, the ground state is $^2A_{1g}$. Further tetragonal cupric complexes with D_{4h} generally have g_{11} (corresponding to the magnetic field along the Z axis of the complexes) $> g_{\perp} > 2.04$ have the ground state $d_{x^2-y^2}$ [32-34]. In the present case $g_{11} > g_{\perp} > 2.00$ (4.82 to 3.14 >2.04 > 2.0036) and hence the ground state is $^2B_{1g}$ ($d_{x^2-y^2}$).

Using the above data, a new parameter G [35] is defined as $G = \frac{g_{11} - g_e}{g_{\perp} - g_e}$ is nearly 8.0. If G value falls in between 3 and 5, the unit cell contains magnetically non-equivalent ions. If G value is less than 3, the exchange coupling among the magnetically non equivalent Cu(II) ions in the unit cell is not very strong. If G is greater than 5, a strong exchange coupling takes place among the magnetically non equivalent Cu(II) ions in the unit cell.[36-39]. In the present case G is nearly 8.0 which indicates that the unit cell contains magnetically non-equivalent ions and the coupling is very strong. In this, the area ratio of $\frac{g_{\perp}}{g_{11}}$ is always equal to 1.65. Thus the Cu^{2+}/Fe^{3+} cation ratio of octahedral site to tetrahedral site in all compositions remains 1.65 and is equal to XRD values. Further increase in temperature (from 170 K to 300K) caused merger of hyperfine lines and gives only resonant line. Single EPR line is noticed due to high concentration Cu in the compound. Since the compound contains high content of copper the hyperfine lines could not be resolved due to dipolar-dipolar broadening. Further no EPR signal is noticed due to iron because the Al^{3+} ions are dominated by Fe^{3+} ions in both the sites.

(iv) No EPR spectra of $(Cu_{0.90}Zn_{0.10})(Al_{0.90}Fe_{1.10})O_4$ recorded from 95K to 300K is noticed. The transition metal ion with spin S = 1 do not exhibit EPR spectra at normal temperatures. In the binuclear complexes, two spins in the s =½ of two adjacent Cu(II) ions are coupled via a bridging ligand such as oxygen and hence total spin becomes S=1 and hence does not give EPR spectrum. This results in a ferromagnetic behaviour. The ferromagnetism is represented by a positive 2J exchange interaction value (S=1 triplet ground state, S=0 singlet first excited state). At room temperature one can see S=1 signals when (S=0 EPR shows no signal.). The EPR spectra of the isolated Cu(II) containing oxygen ligands show three signals which are typical for the ferro-magnetically coupled Cu(II) centers with spin S=1 in the X band frequency region [31]. This is also not noticed because the compound may exhibit high ferrimagnetism.

3.3 Z-scan measurement results

We tried fitting the measured z-scan data to different nonlinear transmission equations, and the best fit was obtained for a combined process of saturable absorption and effective two-photon absorption (2PA). Fig 5 shows the measured z-scan curves along with the numerical fits. The effective nonlinear absorption coefficient in the present case is given by $\alpha(I) = \frac{\alpha_0}{1+\frac{I}{I_Z}} + \beta I$. Where α_0 is the unsaturated linear absorption coefficient at the wavelength of excitation, I is the input laser intensity (fluence divided by laser pulse width), I_s is the saturation intensity, and β is the effective 2PA coefficient. The corresponding propagation equation to find the transmitted intensity for a given input intensity is given by, $\frac{dI}{dZ^2} = -\left(\frac{\alpha_0}{1+\frac{I}{I_Z}} + \beta I\right) l$

Here $Z^{'}$ indicates the propagation distance within the sample. By solving the above equation β and I_s values for each sample were calculated.

The effective 2PA coefficients are found to be 9×10^{-11} m/W, 7.35×10^{-11} m/W, 7.2×10^{-11} m/W, and 6.3×10^{-11} m/W for x=0.15, 0.45, 0.75 and 0.90 respectively. (The corresponding saturation intensities are 4×10^{13} W/m^2, 2.7×10^{13} W/m^2, 2.3×10^{13} W/m^2,

and 9.95×10^{12} W/m^2 respectively). In comparison, the effective 2PA coefficient values are of the same order as those measured in certain organic Schiff base complexes [40], copper nano-composite glasses [41] and Bi nanorods [42]. The increasing opacity of these samples with input laser fluence shows that these materials are potential materials for optical limiting applications, by which a sensitive detector or human eye can be protected from accidental exposure to intense laser radiation.

4. Conclusions

1. Ferrite compound is synthesized by standard solidstate route method shows crystallinity.
2. XRD results suggest that a higher content of Cu result in the substitution of octahedral sites compared to tetrahedral sites. Further several crystal parameters are evaluated which are coinciding with TEM and SAED results.
3. TEM images shows that the basic unit is composed of both tetrahedral and octahedral geometries and joined together to build the unit cell. TEM pictures are clearly shows both octahedral and tetrahedral forms agglomerated with different sizes with different Al/Cu concentration. The SAED picture indicating that the best crystallinity is noticed at higher Cu/Al concentration.
4. EPR results suggesting that doping of higher amounts of Cu, Al could not altered the ferromagnetic behaviour at room temperature. At low temperatures the compound show both ferromagnetic and paramagnetic nature. This property is useful in several industrial applications. At low Cu concentration, the EPR spectrum is dominant due to iron and at higher Cu concentration the spectrum is due to copper. At very high Cu content no EPR signal is noticed indicating the synthesized nano ferrite is high in ferromagnetic nature.
5. Nonlinear optical transmission measurements employing 5 ns laser pulses at 532nm indicate that these ferrites are potential materials for optical limiting applications.
6. The synthesized material is a nano-structured mixed spinel type ferrite which may have applications in high frequency devices as well as solar cell application.

References

[1] W.E.Ford ,"A Text Book of Mineralogy"4th Edn.,Wiley Eastern Ltd., New Delhi, pp.488 (1989).

[2] S. Son and M. Taheri, E. Carpenter and V. G. Harris, M. E. McHenry, J. Appl. Phys., **91** (2002).

[3] Dhiman,1 S. P. Taneja,2 and V. R. Reddy, Advances in Condensed Matter Physics Volume **2008**, Article ID 839536, 7 pages doi:10.1155/2008/839536.

[4] J.Smith and H.PJ. Wijn, Ferrites (Philips Technical Library Eindhoven, (1959)

[5] C. Upadhyay, H. C. Verma, C. Rath, et al., "Mossbauer studies of nanosize $Mn_{1-x}Zn_xFe_2O_4$," *Journal of Alloys and Compounds,***326** (2001) 94–97.

[6] E. E. Sileo, R. Rotelo, and S. E. Jacobo, "Nickel zinc ferrites prepared by the citrate precursor method," *Physica B,***320** (2002) 257–260.

[7] R. A. Dunlap, A. Alghamdi, J. W. O'Brien, and S. J. Penney, "A Mossbauer effect investigation of superparamagnetic behavior in ball milled Mn-Zn ferrites," *Journal of Alloys and Com- pounds,***365** (2004) 84–88.

[8] Q. A. Pankhurst, J. Connolly, S. K. Jones, and J. Dobson, "Applications of magnetic nanoparticles in biomedicine," *Journal of Physics D,***36** (2003) R167–R181.

[9] R. Jurgons, C. Seliger, A. Hilpert, L. Trahms, S. Odenbach, and C. Alexiou, "Drug loaded magnetic nanoparticles for cancer therapy," *Journal of Physics: Condensed Matter,***18** (2006) S2893–S2902.

[10] J.L.Dormann and M.Nogues, J.Phys. Condens. Matter. **2** (1990) 1223.

[11] C.G. Whinfrey, D.W. Eckart and A.Taybev, J.Am.Chem. Soc.82(1960) 2695-97.

[12] Gopathi Ravi Kumar, Katrpally Vijaya Kumar, Yarram Chetty Venudhar, "Synthesis, Strutural and Magnetic properties of Copper substituted Nickel ferrites by Sol-Gel Method", Materials Science and Applications, **3** (2012) 87-91.

[13] B. D. Cullity, *Elements of X-ray Diffraction,* 2nd Edn., Addison-Wesley, New York, (1978) pp. 101–102.

[14] K. P. Thummer, M. C. Chhantbar, K. B. Modi, G. J. Baldha, and H. H. Joshi, "Localized canted spin behaviour in Znx $Mg_{1.5-x}$ $Mn_{0.5}$ FeO_4 spinel ferrite system," *Journal of Magnetism and Magnetic Materials,***280** (2004) 23–30.

[15] A. Rais, A. M. Gismelseed, and I. A. Al-Omari, "Cation distribution and magnetic properties of nickel-chromium ferrites $NiCr_x$ Fe_{2-x} O_4 ($0 \leq x \leq 1.4$)," *Physica Status Solidi B,***242** (2005) 1497–1503.

[16] S. Singhal, J. Singh, S. K. Barthwal, and K. Chandra, "Preparation and characterization of nanosize nickel-substituted cobalt ferrites (Co_{1-x} $Ni_xFe_2O_4$)," *Journal of Solid State Chemistry,***178** (2005) 3183–3189.

[17] E. Wolska, E. Riedel, and W. Wolski, "The evidence of $Cd_x^{2+}Fe_{1-x}^{3+}[Ni_{1-x}^{2+}$ $Fe_{1+x}^{3+}]O_4$ cation distribution based on X-ray and Mo¨ssbauer data," *Physica Status Solidi A,* **132** (1992) K51–K56.

[18] B. P. Ladgaonkar and A. S. Vaingankar, "X-ray diffraction investigation of cation distribution in Cd_x Cu_{1-x} Fe_2 O_4 ferrite system," *Materials Chemistry and Physics,***56** (1998) 280–283.

[19] A.A. Pandit, A. R. Shitre, D. R. Shengule, and K. M. Jadhav, "Magnetic and dielectric properties of Mg_{1+x} Mn_x ,Fe_{2-2x} , O_4 ferrite system," *Journal of Materials Science,* **40**,(2005) 423–428.

[20] R G. Kulkarni, B. S. Trivedi, H. H. Joshi, and G. J. Baldha, "Magnetic properties of copper ferrite aluminates," *Journal of Magnetism and Magnetic Materials,***159** (1996) 375– 380

[21] J.M. Hatings and L. M. Corliss, "Neutron diffraction study of manganese ferrite," *Physical Review,***104** (1956) 328–331 Advances in Condensed Matter Physics 7

[22] G. A. Sawatzky, F. Van der Woude, and A. H. Morrish, "Note on cation distribution of $MnFe_2O_4$," *Physics Letters A,* **25 (1967)**147–148.

[23] F. S. Li, L. Wang, J. B. Wang, et al., "Site preference of Fe in nanoparticles of ZnFe2 O4," *Journal of Magnetism and Magnetic Materials,***268** (2004)332–339.

[24] T.E. Quickel, V.H.Le, T.Brezesinski, S.H.Tolbert, Nano Letters **10** (2010) 2982- 2988.

[25] Y.Qi, Y.Yang, X.Zhao, X.Liu,P.Wu, F.Zhang, S.Xu, *Particuology,***8** (2010) 207-

211.

[26] N.R. Pawaskar,S.D. Sathaye,M.M. Bhadbhade and K.R. Patil, *Mater. Res. Bull.* **37** (2002) 1539.

[27] Q. Wang, H. Yang, Jiunlin Shi, and Guangtian Zou, *Mater. Res. Bull.* **36** (2001) 503.

[28] P.Sambasiva Rao and S.Subramanian, *Mol.Phys*., **54** (1985) 415

[29] R.W. Kedzie and M.Kestigan, *Appl. Phys. Lett*. **3** (1963) 86.

[30] A.B. Vassilikon-Dova and G.Lehman, *Phys.Chem. Minerals*, **15** (1988) 559.

[31] S. S. Ata-Allah and M. Kaiser, "Cation distribution, hyperfine parameters and conduction mechanism in the ferrimagnetic system $Cu_{0.5}Co_{0.5}Ga_xFe_{2-x}O_4$," *Physica Status Solidi B* **242** (6) (2005) 1324–1335.

[32] E.L. Solomon and D.L. Michael, " The proceedings of the first International Conference on The chemistry of the copper and zinc triads", Uni. of Edinburgh, U.K.12 (1992).

[33] A.A. Gewirth, S.L. Colien, H.J.Schugar and E.I. Solomon, *Inorg. Chem.* **26** (1987)1133.

[34] D.Attanasio, I.Collamati and C.Ercolani, J.Chem.Soc. *Dalton Trans.* **1319** (1974).

[35] M.Massceli, G.Ponticelli, V.B.Addepalli and V.G.Krishan, *J.Mol.Struct*, **48** (1978) 55.

[36**]** I.M.Procter, B.J. Hathaway and P.Nicholls, *J.Chem.Soc.A* **1678** (1968).

[37] A.A.G. Tomlinson and B.J. Hathaway, *J.Chem. Soc.A*, **1685**, (1968)1905.

[38] M.J. Bew, B.J. Hathaway and R.J. Faraday, *J.Chem. Soc.A* **1229** (1972)

[39] D.C.Billing, B.J.Hawthaway, *J.Chem. Soc.A*, **1516** (1969)

[40] H.C. Sampath Kumar, B.R. Bhat, B.J. Rudresha, R. Ravindra, Reji Philip, *Chemical Physics Letters* **494** (2010) 95.

[41] B.Karthikeyan, M.Anija, Suchand sandeep C.S., Muhammad Nadeer T.M., Reji Philip, *Optics Communications* **281** (2008) 2933.

[42] S.Sivaramakrishnan, V.S.Muthukumar, S.Sivasankara Sai, K.Venkataramanaiah, J.Reppert, A.M. Rao, M.Anija, Reji Philip, N.Kuthirummal, *Applied Physics Letters* **91** (2007) 093104.

List of Tables.

List of Figures

Table 1

x	$CuCl_2$ $2H_2O$ (170.48)	Zn granules (65.38)	Fe $(NH_4)_2(SO_4)_2$ $6H_2O$ (392.16)	$Al_2(SO_4)_3.18H_2O$ (666.42)
0.15	0.4024	55.573	12.9898	3.7048
0.45	1.2072	35.959	10.8834	11.1144
0.75	2.0120	16.345	8.7769	18.524
0.90	2.4145	6.538	7.7237	22.2288

Cu = 63.546 ; Zn = 65.38 ; Fe = 55.85 ; Al = 26.982 ; O =16; H =1.

Table 2

Composition (x)	Lattice constat (Å) a_o	Mass of the ferrite	X ray density (d_x) gm/cm^3	Grain size (nm)	
				XRD	TEM
0.15	8.396	233.4758	5.2396	50	70
0.45	8.699	227.2484	4.587	50	60
0.75	8.753	218.0279	4.3188	43	45
0.90	8.890	213.4167	4.0345	34	35

Table -3

Composition	X-ray intensity			Cation distribution	Fe^{3+} B site/A site
	I_{220}/I_{440}	I_{422}/I_{440}	I_{440}/I_{400}		
$Cu_{0.15}Zn_{0.85}Al_{0.15}Fe_{1.85}O_4$	1.2375	0.2951	2.2453	$Cu_{0.15}Zn_{0.85}Al_{0.15}Fe_{1.85}O_4$	1.56
$Cu_{0.90}Zn_{0.10}Al_{0.90}Fe_{1.10}O_4$	0.1917	0.2880	0.1142	$Cu_{0.15}Zn_{0.85}Al_{0.15}Fe_{1.85}O_4$	1.50

Table-4.

Grain size (nm)				Crystal plane d-spacing (nm)			
Concentration (x)							
0.15	0.45	0.75	0.90	0.15	0.45	0.75	0.90
			31.18	3.61			3.59
			32.16	3.61	3.93	3.97	
			39.18	3.61	4.13		
		62.18	63.65	4.36	4.26	4.29	4.21
		78.90	65.82	4.96		5.09	5.03
			94.14		5.21(2)		
120.39		110.35	115.18(2)	6.32		6.08	6.07
130.39		126.19		6.38			
132.49		139.28		6.47			
148.94	143.02	198.48		6.49			
165.73				6.54			
173.23				7.19	7.02	6.93	6.60
	213.81				7.34	7.32	7.06
	264.30						7.92
	316.20						9.58

Table 5

Parameter	Temperature (K)								
	95	120	145	170	195	220	245	270	300
g_1	4.82	4.66	4.36	4.02	3.75	3.46	3.38	3.22	3.14
B(Gauss)	1400	1450	1550	1680	1800	1950	2000	2100	2150
g_2	2.04	2.04	2.04	2.04	2.04	2.04	2.04	2.04	2.04
B(Gauss)	3315	3315	3315	3315	3315	3315	3315	3315	3315

A site area	10	19	18	18	17	16	8	9	6
B site area	16	32	30	30	28	26	13	15	10
B site/A site	1.60	1.68	1.67	1.67	1.64	1.63	1.63	1.67	1.66

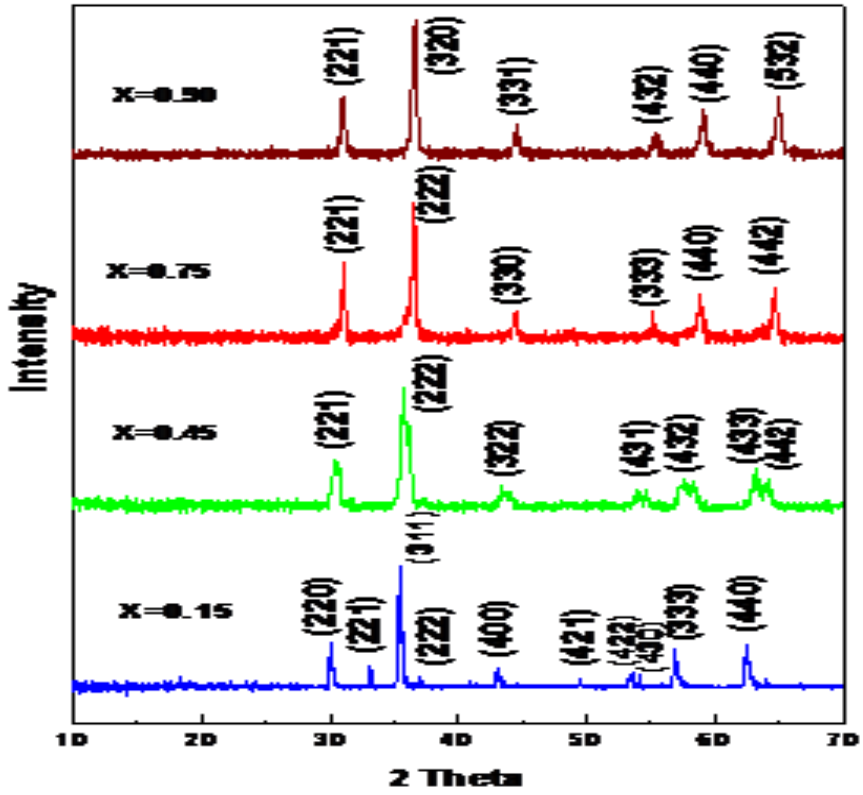

Fig. 1 XRD spectrum of $(Cu_xZn_{1-x})(Al_xFe_{2-x})O_4$

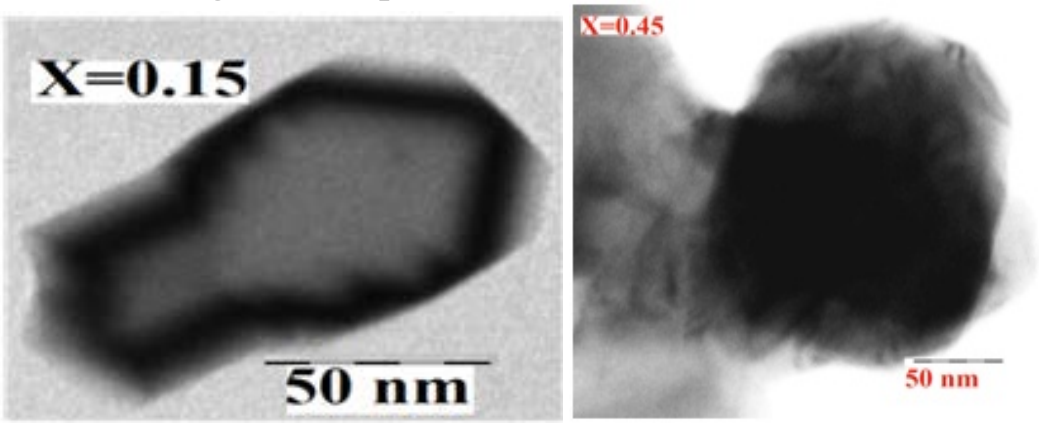

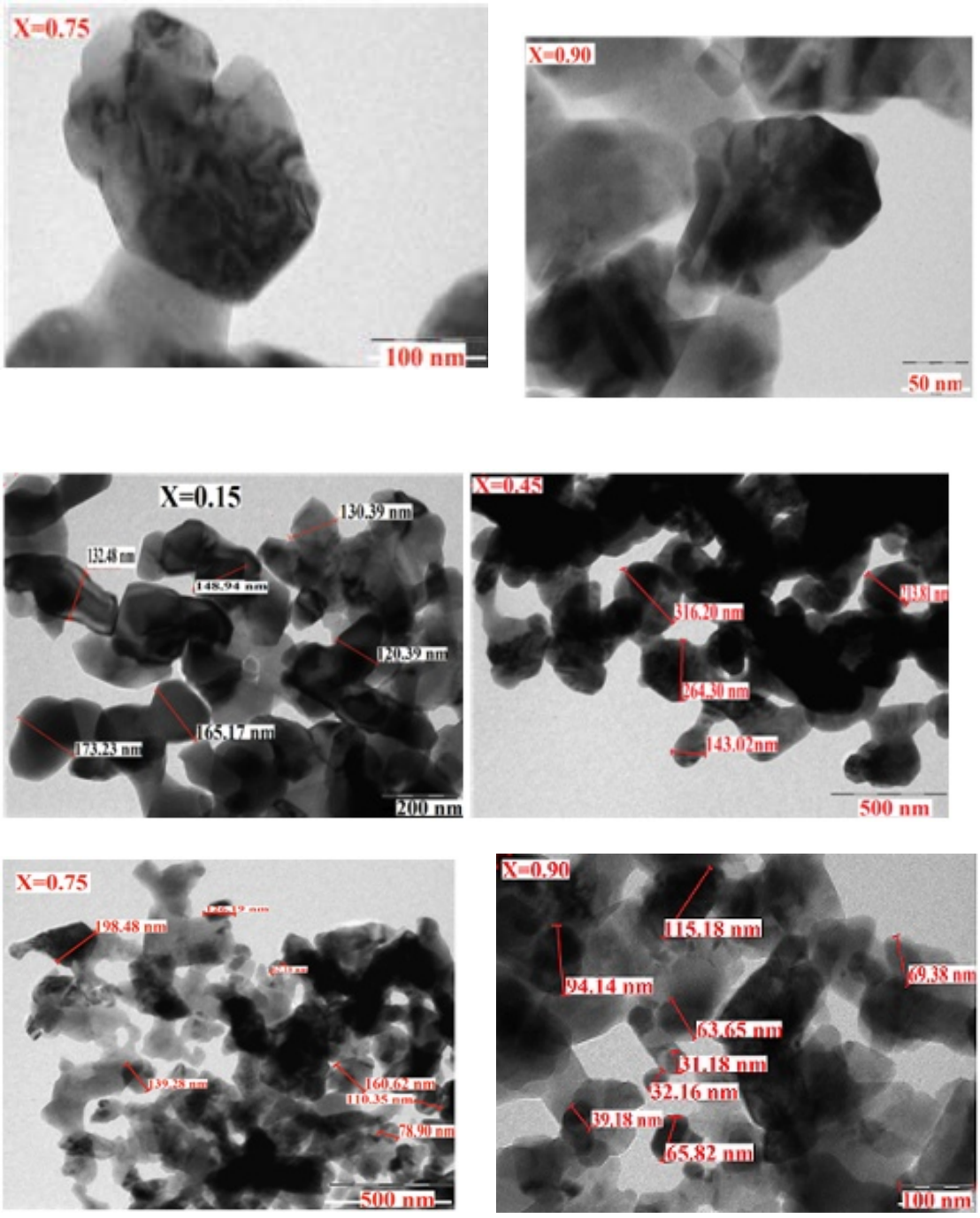

Fig. 2 TEM images of $(Cu_xZn_{1-x})(Al_xFe_{2-x})O_4$

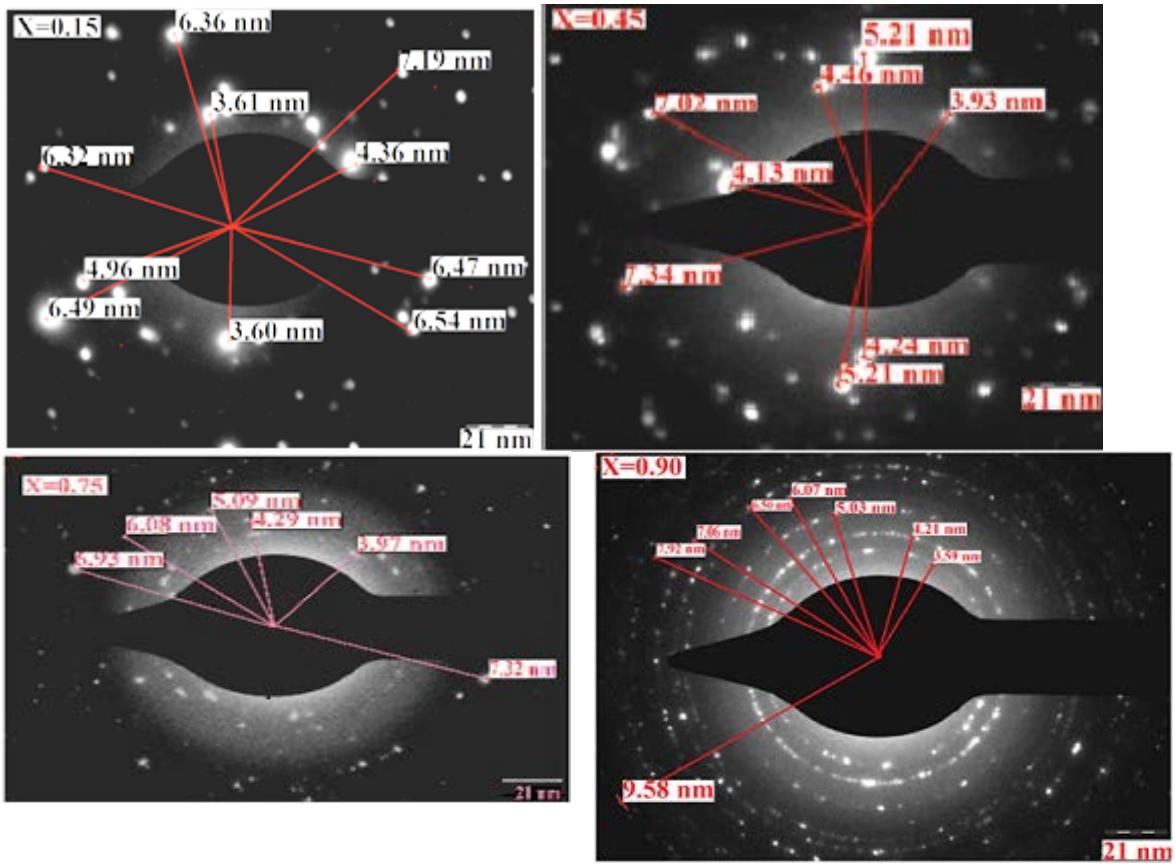

Fig. 3 SAED pattern of $(Cu_xZn_{1-x})(Al_xFe_{2-x})O_4$

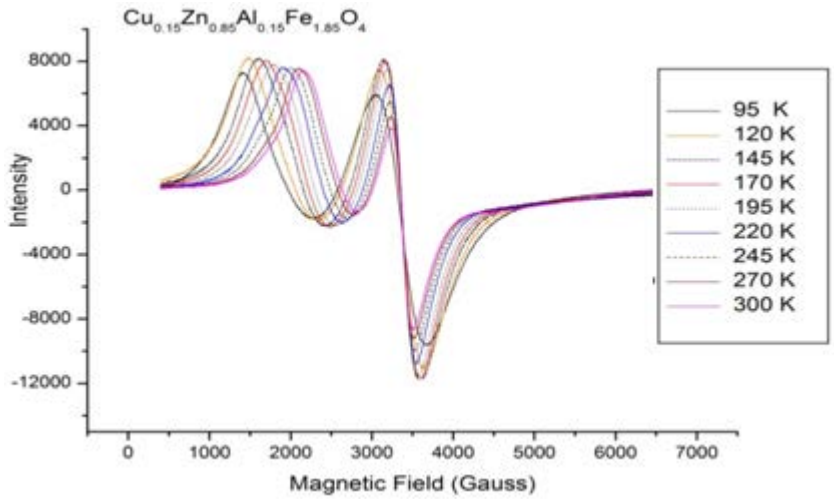

Fig. 4(a) EPR spectrum of $(Cu_{0.15}Zn_{0.85})(Al_{0.15}Fe_{1.85})O_4$

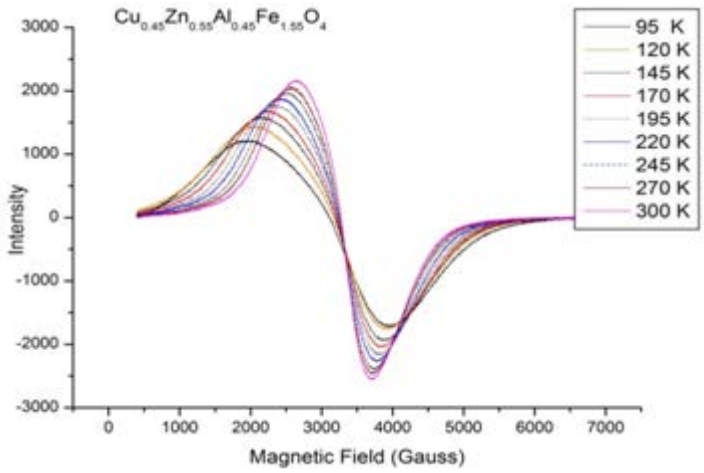

Fig. 4(b) EPR spectrum of $(Cu_{0.45}Zn_{0.55})(Al_{0.45}Fe_{1.55})O_4$

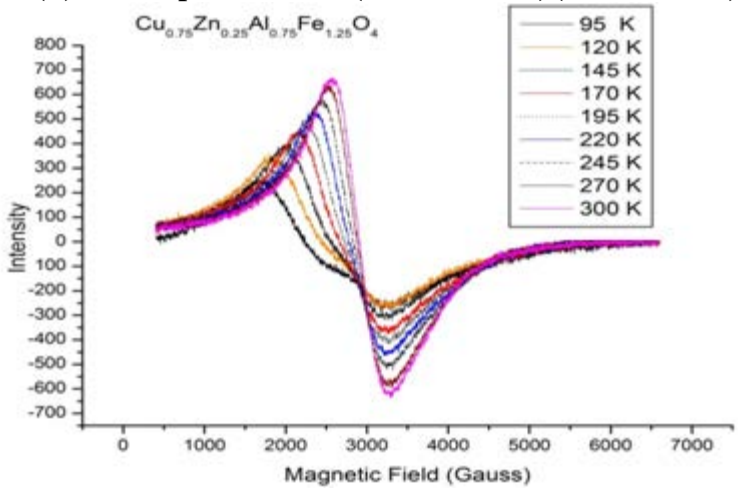

Fig. 4(c) EPR spectrum of $(Cu_{0.75}Zn_{0.25})(Al_{0.75}Fe_{1.25})O_4$

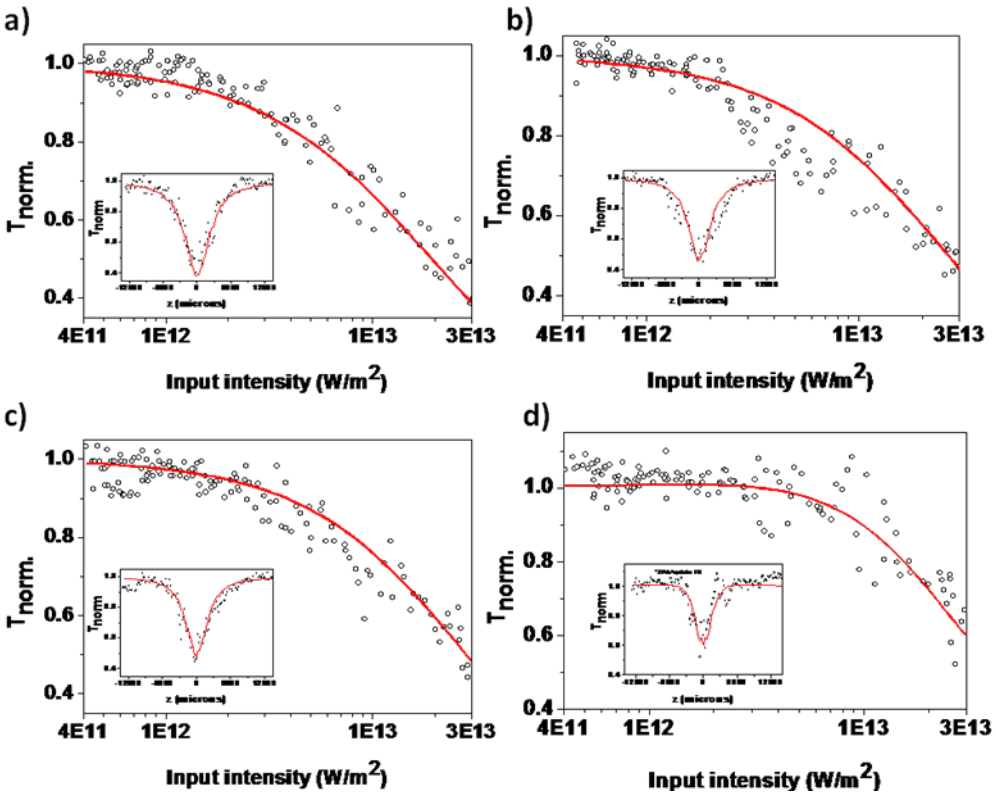
a)
b)
c)
d)
Tnorm.
1.0
0.8
0.6
0.4
4E11
1E12
1E13
3E13
Input intensity (W/m2)
z (microns)

Fig. 5.